TAO, Vol. 9, No. 1, 31-50, March 1998

Strain Accumulation in Southwestern Taiwan

Shui-Beih Yu[1] and Horng-Yue Chen[1]

(Manuscript received 29 August 1997, in final form 7 January 1998)

ABSTRACT

The 1990-1997 annually surveyed GPS data from 36 stations and continuous data from 3 permanent stations in southwestern Taiwan are utilized to study the spatial and temporal variations of crustal strain in the area. Moderate to remarkable contraction rates of 0.48-2.01 μstrain/yr in 91°-135° are observed in the vicinity of the Chukou fault (CKF). The contraction rates decrease toward either the east or the west. Along the surface trace of the CKF, the strain rates of the northern segment are approximately at the same level, while that for the central and southern segments clearly increase toward the south. The temporal variations of crustal strain near the CKF are quite uniform during the period from 1990 to 1997. Analyzing the repeated GPS data of a dense profile across the central segment of the CKF from 1993 to 1997, it is found that the E-W shortening is distributed at several places and is not solely due to slip along the CKF. The east velocity components relative to Penghu increase dramatically from 2.6 mm/yr near the western coast to 39.9 mm/yr in the foothill region to the east of the CKF. These results indicate that crustal strain is accumulating rapidly and that there is a very high possibility of a forthcoming major earthquake in the Chianan area. The extremely high strain rates in the southern segment of the CKF may be caused by the aseismic slip on the fault, as the seismic activity here is insignificant.

(Key words: Crustal strain, GPS survey, Active fault, Southwestern Taiwan)

1. INTRODUCTION

Since the beginning of the twentieth century, fifteen earthquakes with magnitudes of more than 6 have occurred in the Chianan (Chiayi-Tainan) area of southwestern Taiwan (Cheng and Yeh, 1989). However, sinice the 1964 Paiho earthquake (M_L=6.5) there have been no more $M_L \geq 6$ earthquakes in this region. Figure 1 shows the seismicity in southwestern Taiwan during the period from 1973 to 1996, as located by the Taiwan Telemetered Seismographic Network (TTSN) and the Central Weather Bureau Network (CWBN). These small to moderate

[1]Institute of Earth Sciences, Academia Sinica, P.O. Box 1-55, Nankang, Taipei, Taiwan, ROC

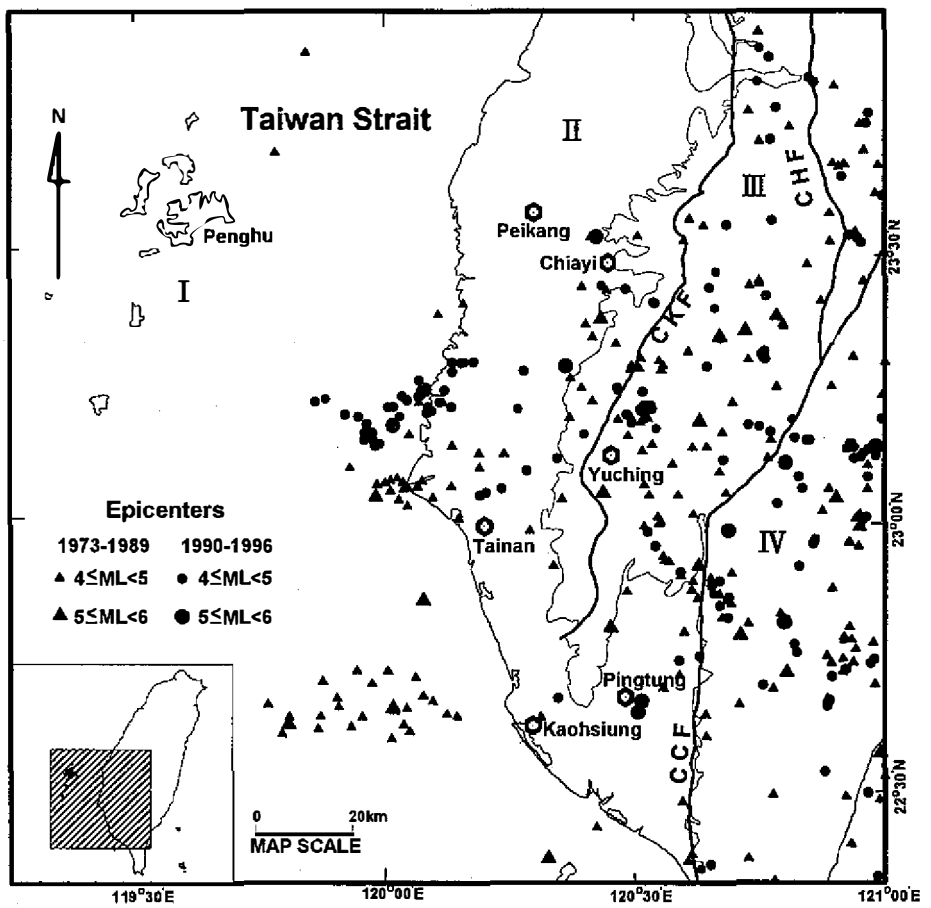

Fig. 1. Seismicity (1973-1996) and geologic provinces in southwestern Taiwan. Triangles and circles are epicenters of earthquakes occurred during 1973-1989 and 1990-1996, respectively. Geologic provinces, I: Penghu Island Group, II: Coastal Plain, III: Western Foothills, IV: Central Range. Major thrust faults, CKF: Chukou fault, CHF: Chuchih fault, CCF: Chaochou fault.

earthquakes ($4 \leq M_L 6$) are distributed across a broad area. It is difficult to relate the seismicity to the activities of any particular faults. Nevertheless, the Chianan area is undoubtedly a highly active seismic region.

The Global Positioning System (GPS) is a satellite-based navigation system with a constellation of 24 satellites in orbits of 20,000 km in altitude. By receiving the signals from GPS satellites at several sites simultaneously, the 3-dimensional relative position of these sites can be precisely determined. An islandwide "Taiwan GPS Network" was established in 1989 and has been surveyed annually since 1990. Yu and Chen (1994) analyzed the 1990-1994 observed GPS data in southern Taiwan to study the crustal deformation caused by the arc-conti-

nent collision. Based on the changes of baseline lengths from repeated GPS survey before 1995, Yu *et al.* (1997) estimated the velocity field of stations for the entire "Taiwan GPS Network" and discussed its tectonic implications.

In this paper, the annually surveyed GPS data in southwestern Taiwan from 1990 to 1997 are utilized to study the spatial variation and accumulation of crustal strain. The repeated GPS data of a fault-crossing dense profile from 1993 to 1997 are also analyzed to assess the possibility of a forthcoming major earthquake in the Chianan area.

2. GEOLOGICAL SETTING

Taiwan is a young orogenic belt. It is usually divided into several geologic provinces which trend mainly north-northeast (Ho, 1982, 1986). This study area covers the following geologic provinces: the Penghu Island Group (I), the southern portions of the Coastal Plain (II), the Western Foothills (III) and the Central Range (IV), as shown in Figure 1. The little-disturbed Penghu Island Group in the Taiwan Strait is covered mostly with Miocene flood basalts. The Coastal Plain is composed of Quaternary alluvial sediments and well-bedded, but poorly consolidated clastic deposits (Ho, 1986). The Western Foothills province consists of a thick sequence of shallow marine to shelf clastic sediments from the late Oligocene, Miocene, to Early Pleistocene. The Central Range is further divided into two parts. The western flank and high ridges are underlain by a weakly metamorphosed Cenozoic argillite-slate series, while the eastern flank is composed of a pre-Tertiary basement complex which has been affected by Neogene greenschist facies and higher grades of polyphase Mesozoic-Cenozoic metamorphism.

The Neogene sediments under the basalt in the Penghu Island Group and Taiwan Strait are generally low-dipping to nearly flat and possibly lie on Mesozoic to Paleocene basement rocks (Chou, 1969; Chiu, 1973). Beneath the alluvial cover of the Coastal Plain, several gently folded anticlinal structures in the Neogene rocks were found by geophysical surveys and test drilling. The Peikang basement high extending from Peikang in southwestern Taiwan, westerly to the Penghu Islands is also recognized. It is bounded to the east and south by the Yichu marginal fault and may be an elevated part of the basement resulting from differential erosion or uplifting (Meng, 1967; Ho, 1982).

The rocks in the Western Foothills were deformed by a combination of folds and thrust faults which trend mainly northeast or north and dip toward the east or southeast (Ho, 1976; Suppe, 1980). The intensity of deformation decreases from the eastern foothills toward the western rolling hills. Many of the faults are low-angle or bedding thrusts formed parallel to the folds. Each succeeding southeast-dipping thrust faults overrides the one northeast of it resulting in a characteristic imbricate fault system (Ho, 1982). The Chukou fault (CKF) shown in Figure 1 is one of the major thrust faults in this geologic province. This fault trends sinuously as inferred from rock exposures. It is low-angled, dipping to the east, and may become a sole thrust at depth (Tsan and Keng, 1968).

East of the Western Foothills, the submetamorphic argillaceous belt of the Central Range is encountered. Both open and tight folds are presented and dissected by a number of thrust faults (Ho, 1975). The Chuchih-Chaochou fault (CHF and CCF in Figure 1) is one of the

boundary faults separating the slate belt and the fold-and-thrust belt of the Western Foothills.

3. GPS MEASUREMENT AND DATA PROCESSING

Most of the 36 annually surveyed GPS stations in southwestern Taiwan have been surveyed 6-8 times between 1990 and 1997. In each survey, 4-12 stations were observed simultaneously with dual-frequency geodetic GPS receivers (Trimble 4000 SST Geodetic IIP and 4000 SSE/SSI Geodetic Surveyor). A station is usually occupied by more than two sessions. Each session is composed of 6-14 h of observations with all available healthy GPS satellites rising higher than 15° above the horizon being tracked. In this area, three permanent stations, Paisha, Penghu (S01R), Pingtung (S23R), and Minhsiung (S103) have been continuously recording since November 1991. They are equipped with the same models of receivers as those used in the epoch field surveys.

The annually surveyed and the continuous GPS data are incorporated and processed with the Bernese GPS software v.4.0 (Rothacher and Mervart, 1996) session by session to obtain the precise station coordinates and baseline vectors. The precise ephemerides provided by Scripps Institution of Oceanography (SIO) of the University of California, San Diego, U.S.A are employed in the processing of the 1992 and 1993 data, while the 1990-1991 data can be only processed with the broadcast ephemerides. Since the beginning of 1994, the official final precise ephemerides distributed by the International GPS Service for Geodynamics (IGS) have been utilized in the GPS data processing.

The ionosphere-free linear combination of observations at the L_1 and L_2 frequencies, L_3, are used to remove the first-order ionospheric effects. An elevation cut-off angle of 20° is imposed to reduce any multipath effects and noise. The tropospheric corrections are calculated based on the modified Hopfield (1971) atmospheric zenith delay model with standard atmosphere. The residual zenith delay, which is the difference between the actual zenith delay and that calculated from a standard atmosphere model, is further estimated once per 6-h observation session in the least-squares adjustment of the carrier phase observations (Brunner and Welsch, 1993).

Analyzing the scatter of GPS measurements taken over 1990-1995 after the linear trend had been removed, Yu *et al.* (1997) concluded that the standard deviations of annually surveyed GPS data in the Taiwan area range from 6 to 10 mm for length, 6 to 11 mm for the north component, 7 to 16 mm for the east component, and 25 to 54 mm for the vertical component for baseline length in the range of 3 to 120 km. It is obvious that the vertical component is the one most poorly determined with GPS. Thus only the changes in horizontal components are utilized to study the horizontal deformation in southwestern Taiwan.

Figures 2-4 show the plots of observed lengths for some baselines as a function of time. The slope of straight line best fitting to each of the data sets gives an estimate of the average rate of length changes. A positive value of length rate indicates an extension, while a negative rate denotes a shortening. The approximate length and azimuth for each baseline are also shown in the figures. The baselines in the Coastal Plain area with azimuths of 79°-128° give shortening rates of 4.0-10.2 mm/yr (Figure 2). The baselines across the CKF with azimuths 83°-122° have the remarkable shortening rates of 6.3-27.9 mm/yr (Figure 3). On the other

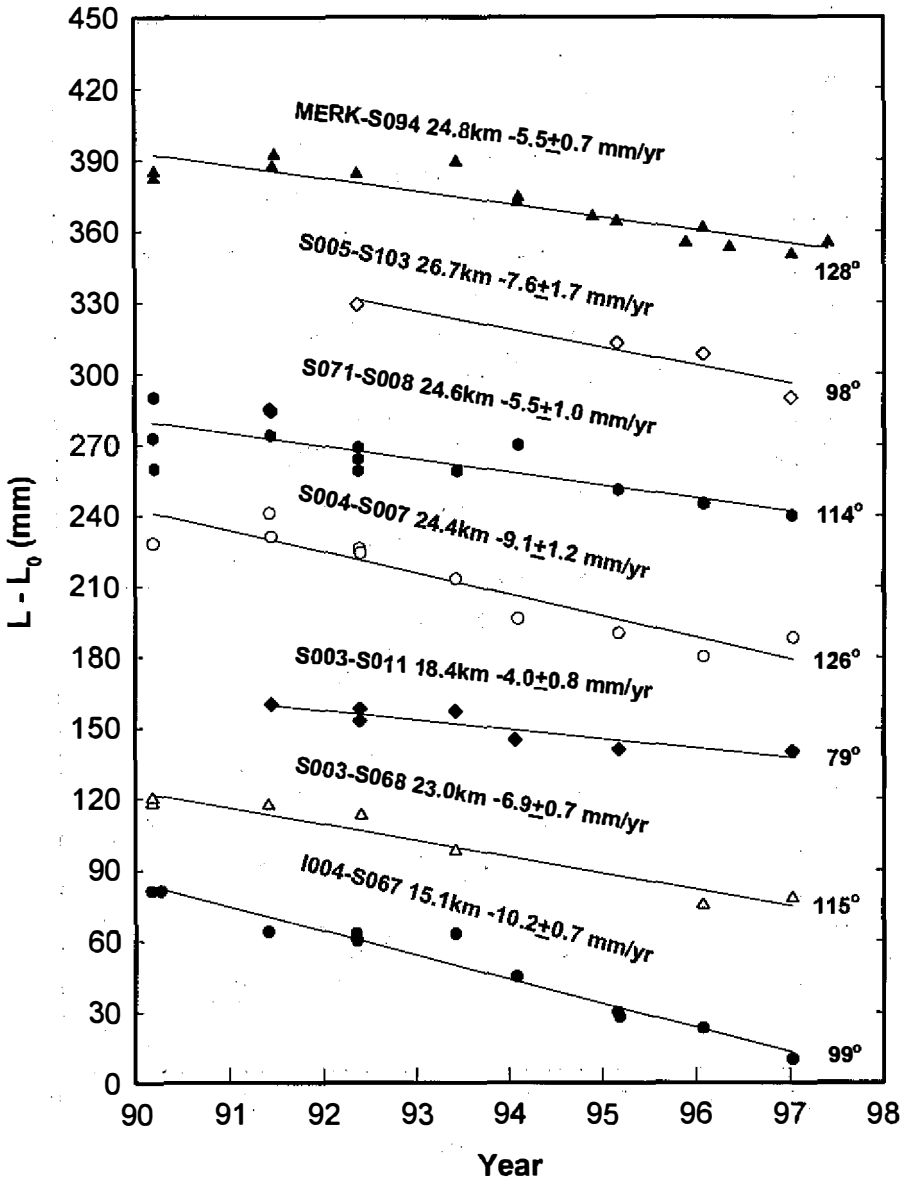

Fig. 2. The observed length L (less a nominal length L_0) plotted as a function of time from 1990 to 1997 for 7 baselines in the Coastal Plain. The straight lines are the best linear fitting. The stations names, length, average length rate and azimuth for each baseline are also shown.

hand, only moderate shortening rates of 4.7-16.4 mm/yr were observed for baselines to the east of CKF with azimuths of 95°-132° (Figure 4). In general, the time variations of baseline lengths are quite uniform during the period from 1990 to 1997.

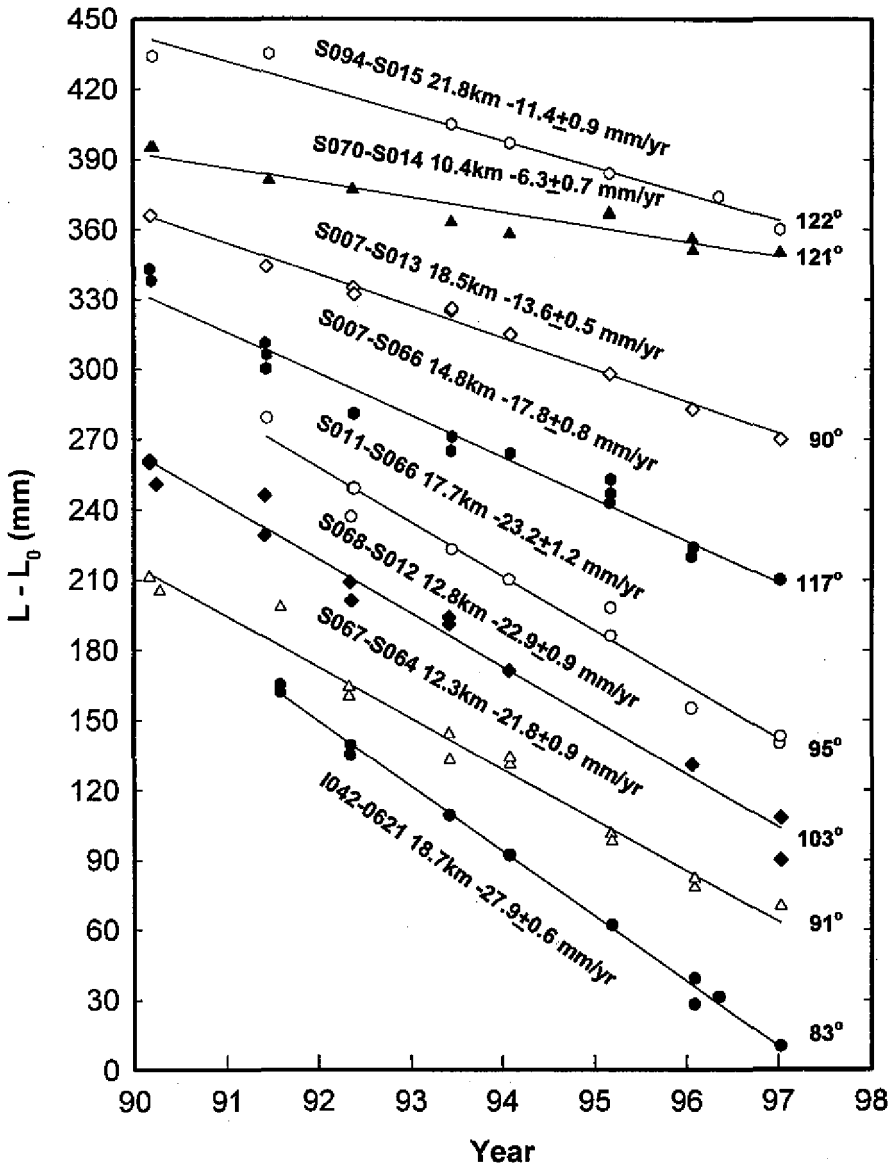

Fig. 3. Same as Figure 2, except for 8 lines across the Chukou fault.

4. CRUSTAL STRAIN

To realize the spatial variation of crustal strain in southwestern Taiwan, the GPS network is divided into 56 triangular subnets as shown in Figure 5, and the strain rates of each triangle are computed. The strain rate for a baseline, $\dot{e}$, is expressed as $\dot{e} = L^{-1}(dL/dt)$, where L is the baseline length and dL/dt is the average rate of length change (Prescott *et al.*, 1979). $\dot{e}$ is related to the surface strain rate tensor, $\dot{E}_{ij}$, by:

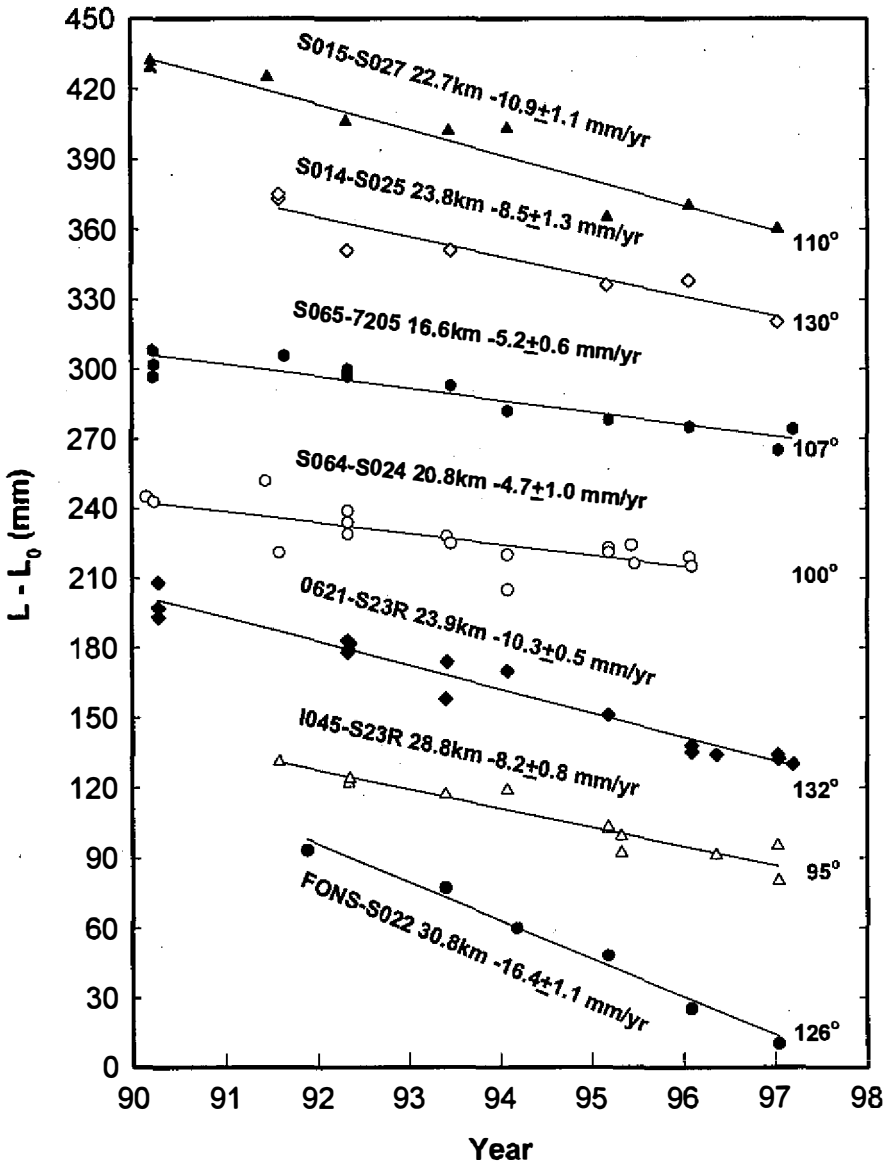

Fig. 4. Same as Figure 2, except for 7 lines to the east of the Chukou fault.

$$\dot{e} = \dot{E}_{11}\sin^2\theta + \dot{E}_{12}\sin 2\theta + \dot{E}_{22}\cos^2\theta \qquad (1)$$

where θ is the azimuth (measured clockwise from the north) of the baseline. The strain rate tensor is referred to a geographic coordinate system with axis 1 directed east and axis 2 directed north. We assume that the crustal strain accumulates uniformly over each subnet and that the rate of strain accumulation is constant over the time period from 1990 to 1997. Three

components of average surface strain rate tensor, $\dot{E}_{11}$, $\dot{E}_{12}$, and $\dot{E}_{22}$ using all of the surveys for each of the 56 subnets are calculated.

The average principal strain rates are then computed from three components of surface strain rate tensor using the following formula :

$$\dot{\varepsilon}_{1,2} = \frac{1}{2}\left(\dot{E}_{11} + \dot{E}_{22}\right) \pm \left[\dot{E}_{12}{}^{2} + \frac{1}{4}\left(\dot{E}_{11} - \dot{E}_{22}\right)^{2}\right]^{1/2} \qquad (2)$$

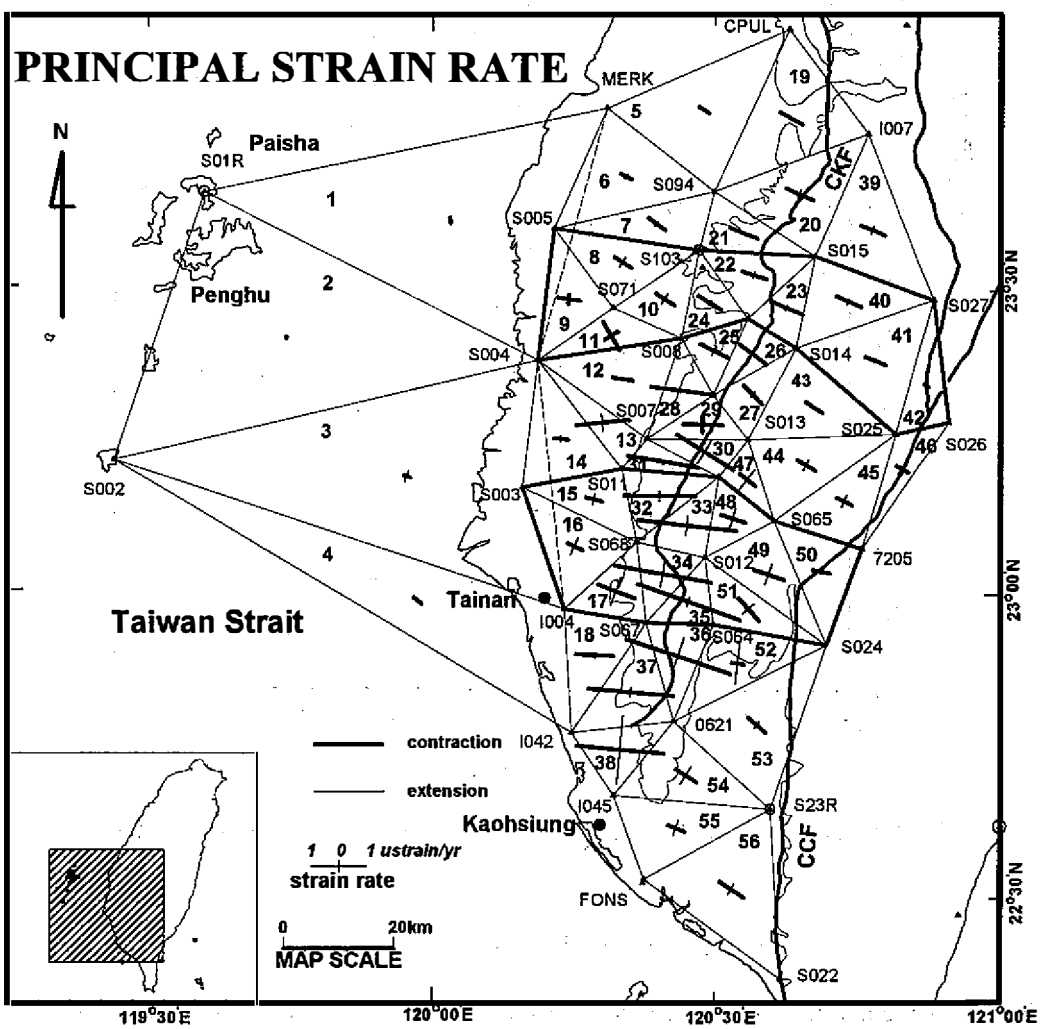

Fig. 5. Principal strain rates for 56 subnets in southwestern Taiwan. Thick line denotes contraction, while thin line represents extension.

where $\dot{\varepsilon}_1$ and $\dot{\varepsilon}_2$ are the algebraically larger and smaller principal strain rates, respectively. The azimuth of $\dot{\varepsilon}_1$, φ, is given by :

$$\varphi = \frac{1}{2}\tan^{-1}\frac{2\dot{E}_{12}}{\dot{E}_{22}-\dot{E}_{11}} \qquad (3)$$

The average principal strain rates for each of the 56 subnets are given in Table 1 and also shown in Figure 5. The uncertainties quoted are ± 1 standard deviation. The strain rates are expressed in microstrain per year (1 μstrain = 10^{-6}). Positive values represent extension, while negative values denote contraction or shortening.

Insignificant or slight deformation are observed in the offshore area between the Penghu Islands and the southwest coast (Nets 1-4). In the Coastal Plain area Nets 5-16 have slight extension rates of 0.01-0.33 μstrain/yr and slight to moderate contraction rates of 0.22-0.97 μstrain/yr. The contractions of these nets are mostly in the E-W to ESE-WNW directions.

Nets 17-38 are located very close or traversing the CKF. Moderate to remarkable contraction rates of 0.48-2.01 μstrain/yr in the directions of 91°-135° (see table 1, φ+90°) are found. Some nets also have significant extension rates of 0.12-1.26 μstrain/yr. Figure 6 shows the spatial variation of $\dot{\varepsilon}_1$ and $\dot{\varepsilon}_2$ for the nets along the surface trace of the CKF. For comparison, the negative values of $\dot{\varepsilon}_2$ have been changed to positive values in Figures 6-7. The distance in the abscissa is measured from the geometric center of Net 19 and approximately parallel to the strike of the CKF. The contraction rates are always higher than the extension rates. Both $\dot{\varepsilon}_1$ and $\dot{\varepsilon}_2$ are clearly increasing toward the south. However, this increasing trend seems not to be

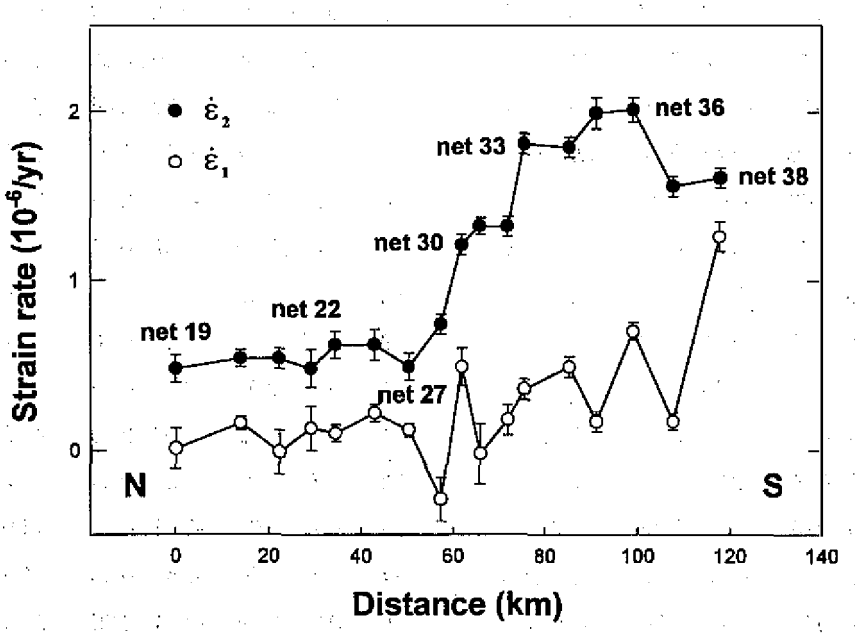

Fig. 6. Spatial variation of principal strain rates along the surface trace of the Chukou fault. The negative values of $\dot{\varepsilon}_2$ are changed to positive values.

Table 1. Principal strain rates of 56 subnets in southwestern Taiwan (1990-1997).

NET	ε_1 (μstrain/yr)	ε_2 (μstrain/yr)	φ (°)	NET	ε_1 (μstrain/yr)	ε_2 (μstrain/yr)	φ (°)
1	0.03±0.01	-0.12±0.04	88.3±5.9	29	-0.29±0.13	-0.74±0.06	1.8±6.9
2	-0.02±0.01	-0.04±0.02	-61.2±40.5	30	0.49±0.11	-1.21±0.06	32.0±3.4
3	0.20±0.03	-0.13±0.02	17.9±3.1	31	-0.02±0.18	-1.32±0.05	9.9±3.9
4	0.07±0.12	-0.19±0.04	40.9±8.6	32	0.18±0.09	-1.32±0.06	0.5±2.4
5	0.01±0.11	-0.22±0.03	32.3±19.2	33	0.36±0.06	-1.82±0.06	6.3±1.7
6	-0.06±0.04	-0.23±0.03	28.2±15.0	34	0.49±0.06	-1.79±0.06	10.0±1.6
7	0.09±0.10	-0.39±0.15	37.1±10.5	35	0.17±0.06	-1.99±0.09	19.7±1.6
8	0.22±0.14	-0.37±0.06	32.5±6.4	36	0.70±0.05	-2.01±0.07	18.5±1.1
9	-0.17±0.05	-0.42±0.09	9.0±9.3	37	0.17±0.05	-1.56±0.06	5.0±1.8
10	0.23±0.08	-0.42±0.07	32.8±8.8	38	1.26±0.09	-1.61±0.06	5.1±1.2
11	-0.30±0.04	-0.60±0.19	59.5±17.9	39	0.16±0.04	-0.48±0.04	22.1±3.3
12	0.06±0.05	-0.38±0.04	8.2±5.2	40	0.10±0.05	-0.48±0.05	24.1±4.3
13	0.31±0.14	-0.97±0.16	-5.3±2.9	41	0.07±0.05	-0.41±0.05	21.5±4.3
14	0.11±0.03	-0.26±0.07	5.8±8.3	42	0.08±0.07	-0.10±0.14	33.1±17.4
15	0.22±0.13	-0.32±0.04	14.4±7.6	43	0.06±0.04	-0.36±0.05	33.1±6.0
16	0.33±0.07	-0.30±0.05	23.7±4.2	44	0.21±0.07	-0.38±0.06	29.1±2.9
17	0.56±0.06	-0.72±0.07	20.3±2.4	45	0.23±0.04	-0.32±0.05	25.3±6.6
18	-0.05±0.03	-0.69±0.06	2.1±5.0	46	0.26±0.03	-0.26±0.23	31.5±9.5
19	0.01±0.12	-0.48±0.08	28.9±6.6	47	0.47±0.10	-0.37±0.08	38.2±5.8
20	0.16±0.04	-0.54±0.05	23.8±3.9	48	0.37±0.06	-0.47±0.08	17.5±3.4
21	-0.01±0.13	-0.54±0.06	21.4±13.2	49	0.39±0.15	-0.58±0.16	18.7±2.1
22	0.13±0.13	-0.48±0.11	17.0±8.7	50	0.09±0.05	-0.32±0.05	11.3±8.2
23	0.10±0.05	-0.62±0.08	22.6±5.7	51	0.29±0.30	-0.56±0.15	48.5±3.0
24	-0.06±0.06	-0.50±0.07	32.3±7.5	52	0.76±0.07	-0.23±0.04	6.7±3.6
25	0.19±0.07	-0.59±0.12	27.3±5.0	53	0.16±0.03	-0.43±0.03	41.0±3.3
26	0.22±0.05	-0.62±0.09	36.3±5.5	54	0.38±0.08	-0.46±0.03	31.9±3.2
27	0.12±0.04	-0.49±0.08	45.5±6.6	55	0.30±0.09	-0.34±0.05	21.8±4.5
28	0.09±0.05	-1.12±0.13	7.9±3.2	56	0.21±0.04	-0.54±0.06	32.8±2.2

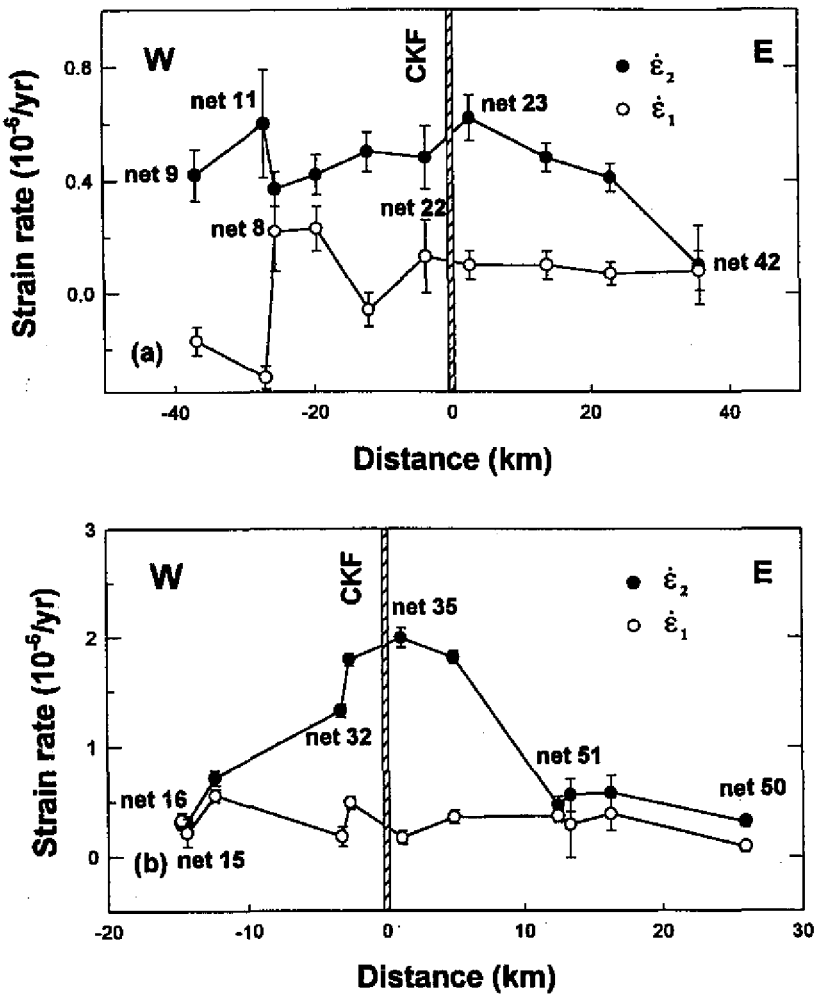

Fig. 7. Two E-W strain rate profiles across the Chukou fault (CKF), (a) Northern profile, (b) Southern profile. The location of two profiles are shown in Figure 5 with thick lines. The negative values of $\dot{\varepsilon}_2$ are changed to positive values.

applicable to the nets north of Net 27. The strain rates of those nets are more or less at the same level.

To the east of the Chukou fault, Nets 39-56 give slight to moderate extension rates of 0.06-0.76 μ strain/yr and contraction rates of 0.10-0.58 μ strain/yr. The directions of contraction are mostly in ESE-WNW to SE-NW. Two E-W trending strain rate profiles are plotted in Figure 7. The abscissas give the projected distance of the geometric center for each net from the CKF. The northern profile includes Nets 8-11, 22-24, and 40-42 (see Figures 5 and 7a), while the southern profile consists of Nets 15-27, 32-35, and 48-51 (see Figures 5 and 7b). Except for Nets 9 and 11, the extension rates, $\dot{\varepsilon}_1$, in both north and south profiles do not vary

significantly with the distance from the CKF. In contrast, the contraction rates, $\dot{\varepsilon}_2$, are increasing toward the CKF. The crustal strains in the northern profile are distributed in a wide zone of probably more than 80 km, while that for the southern profile are concentrated on a narrow zone of about 30 km in width. It is likely there is some aseismic fault-slip in the southernmost segment of the CKF. Otherwise, higher strain rates here may be an indication of a forthcoming major earthquake. Several dense GPS profiles need to be deployed across the CKF and surveyed frequently to resolve the above two issues.

Three components of strain tensor, E_{11}, E_{12}, and E_{22}, for a network at an epoch of annual GPS measurement can also be calculated by only assuming spatially uniform of crustal strain over the network (Prescott *et al.*, 1979). Figure 8 shows the temporal variation of three com-

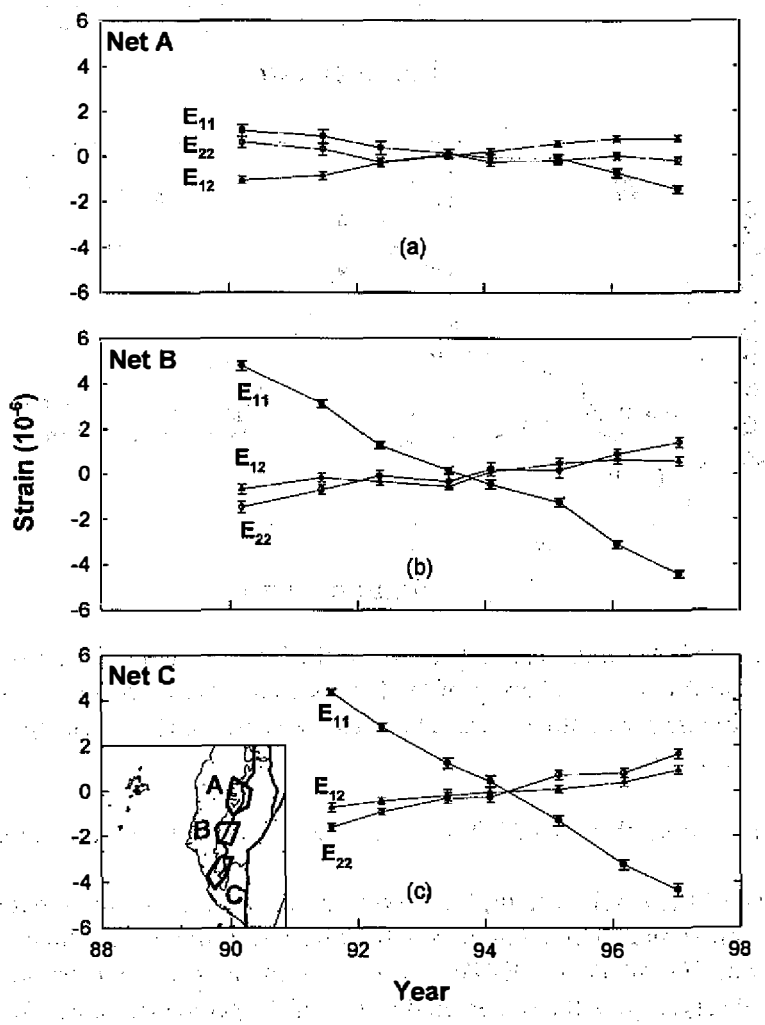

Fig. 8. Temporal variations of three components of strain tensor, E_{11}, E_{12}, and E_{22} for three composite networks along the Chukou fault from 1990 to 1997. (a) Net A, (b) Net B, (c) Net C.

Table 2. Three components of strain rate tensor and principal strain rates of three composite subnets.

NET	E_{11} (μ strain/yr)	E_{12} (μ strain/yr)	E_{22} (μ strain/yr)
A	-0.37±0.04	0.29±0.03	-0.06±0.04
B	-1.29±0.03	0.19±0.03	0.37±0.04
C	-1.63±0.04	0.28±0.04	0.58±0.04

NET	ε_1 (μ strain/yr)	ε_2 (μ strain/yr)	φ (°)
A	0.12±0.03	-0.55±0.03	30.9±2.8
B	0.39±0.04	-1.31±0.03	6.5±1.2
C	0.61±0.04	-1.67±0.05	7.2±0.9

posite networks along the Chukou fault from 1990 to 1997. Net A is composed of Nets 21-26 in Figure 5, while Nets B and C include Nets 30-33 and 36-38, respectively. Since there are more than 7 baselines for each of three composite networks, the standard deviations of strain components at each epoch are also well estimated. The strain components of the three nets have different rates (Table 2). However, their temporal variations are all quite linear. Net B is very close to the epicenter of the 1993 Tapu earthquakes (M_L=5.7), but there is no significant change of crustal strain after the earthquake. This may be due to the deep focal depth (13.5 km) and the fact that the seismic moment was not large enough to cause detectable surface deformation (Shin, 1995).

5. DENSE GPS PROFILE ACROSS THE CHUKOU FAULT

The 14.8 km long baseline S007-S066 across the central segment of the Chukou fault shows a remarkable shortening rate of 17.8 mm/yr (see Figures 3 and 5). In order to realize how is the crustal shortening distributed, a dense GPS profile of 11 new stations was deployed along the highway from Liuchia to Nanhsi in 1993 (Figure 9). This profile was surveyed 5 times between 1993 and 1997.

Table 3 gives the average rates of change of north and east components for each of the successive baselines. An extension is reckoned as positive, while a shortening is negative in value. The uncertainties quoted are ±1 standard deviation of the average rates in units of mm/yr. The lower numbers between two stations are the lengths of baseline components in kilometers. The north components mostly have no significant change. Only two baselines, S007-S083 and S085-S086, reveal slight extension rates of 2.5-2.9 mm/yr. The east components of two baselines, S086-S087 and S066-S092 also have significant extension rates of 11.6 mm/yr

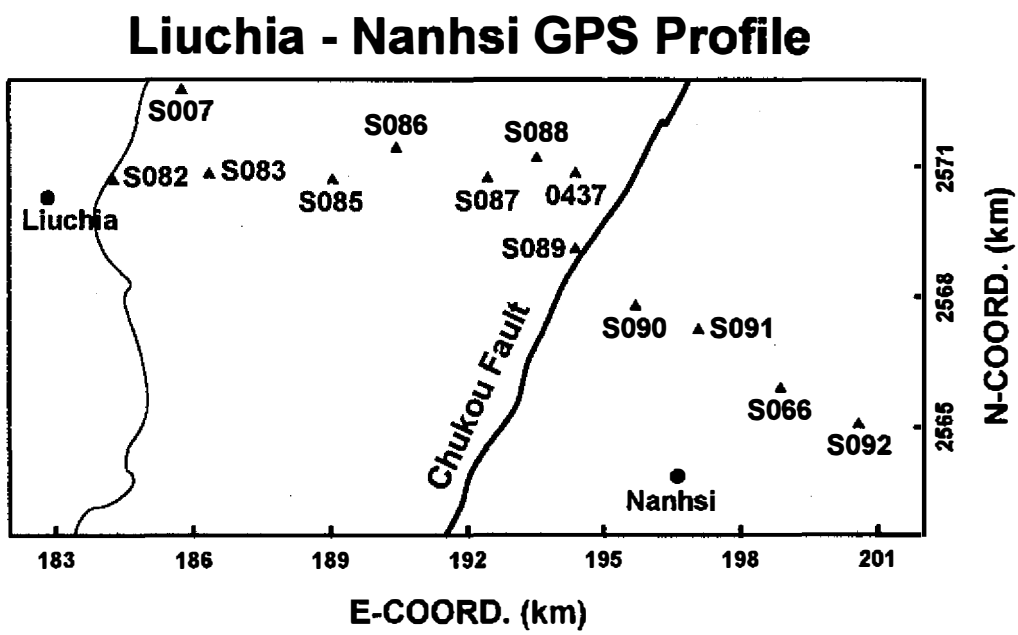

Fig. 9. Liuchia-Nanhsi dense GPS profile. Solid triangles are GPS stations. Thin line is the approximate boundary between the plain area and the rolling hills.

and 2.0 mm/yr respectively. All of the other 10 baselines give slight to moderate shortening of 0.4-7.2 mm/yr in the E-W direction, although four of them are statistically insignificant. These results indicate that the shortening between stations S007 and S066 mentioned previously is distributed at several places and is not solely due to the slip along the CKF (0437-S090). Detailed geological survey is required to identify whether or not the places of high shortening rates are related to slip on the other minor faults. The high extension rate (11.6 mm/yr) between Stations S086 and S087 is not reasonably explained within such an E-W compressional tectonic regime. Since those two stations are situated in a soft mudstone area, it is likely to have been caused by local movement near the sites.

The variance-covariance matrices of daily solutions for the dense profile from 1993 to 1997 are combined with that of the neighboring stations to estimate the station velocities relative to Paisha, Penghu (S01R). The estimated station velocities with east and north components are given in Table 4 and also shown in Figure 10. Except for station S004, all 23 other stations are moving in directions of 270°-298° with rates of 4.5-39.9 mm/yr. The east and north components of velocities for stations in the central part of Figure 10 are plotted as a function of distance from the CKF (Figure 11). The zero point in the abscissa is the location of the CKF and the distances are calculated by projecting the station coordinates to a line perpendicular to the strike (27°) of the CKF. The north components (V_N) are generally in the same level with a small variation for stations in the dense GPS profile. On the contrary the east components (V_E) are increasing dramatically toward the east from 2.6 mm/yr near the coast (S004) to 39.9 mm/yr of foothill region (S065). Although there are local variation of velocities

Table 3. Rates of change on north and east component of baselines in the Liuchia - Nanhsi GPS profile.

1. North component :

S082	$\xrightarrow[2.1]{1.4\pm1.9}$	S007	$\xrightarrow[1.9]{2.5\pm0.3}$	S083	$\xrightarrow[0.1]{1.0\pm0.8}$	S085
S085	$\xrightarrow[0.8]{2.9\pm0.9}$	S086	$\xrightarrow[0.7]{-1.7\pm2.5}$	S087	$\xrightarrow[0.5]{-1.2\pm1.3}$	S088
S088	$\xrightarrow[0.4]{-0.2\pm1.7}$	0437	$\xrightarrow[1.8]{0.6\pm1.2}$	S089	$\xrightarrow[1.3]{1.4\pm0.8}$	S090
S090	$\xrightarrow[0.5]{-2.8\pm1.6}$	S091	$\xrightarrow[1.4]{-1.8\pm0.9}$	S066	$\xrightarrow[0.8]{0.6\pm1.8}$	S092

2. East component :

S082	$\xrightarrow[1.5]{-1.3\pm1.1}$	S007	$\xrightarrow[0.6]{-6.4\pm1.7}$	S083	$\xrightarrow[2.7]{-0.4\pm2.4}$	S085
S085	$\xrightarrow[1.4]{-6.6\pm1.2}$	S086	$\xrightarrow[2.0]{11.6\pm0.8}$	S087	$\xrightarrow[1.1]{-7.2\pm0.9}$	S088
S088	$\xrightarrow[0.8]{-0.5\pm1.1}$	0437	$\xrightarrow[0.1]{-1.3\pm2.8}$	S089	$\xrightarrow[1.3]{-3.0\pm0.8}$	S090
S090	$\xrightarrow[1.4]{-4.0\pm1.1}$	S091	$\xrightarrow[1.3]{-2.1\pm2.4}$	S066	$\xrightarrow[1.8]{2.0\pm0.6}$	S092

* The upper numbers between two stations are rates of baseline component change in units of mm/yr. The lower numbers are the lengths of baseline component in km.

between Stations S083 and S087, this easterly increasing trend of V_E may imply that the crustal strain is accumulating rapidly in the vicinity of the CKF. It gives rise to high potential of generating a major earthquake in the area.

6. CONCLUSIONS

The southwestern part of the "Taiwan GPS Network" has been surveyed annually since 1990. The changes in baseline length from 6-8 times repeated GPS surveys during 1990-1997 are employed to study the spatial variation and accumulation of crustal strain in southwestern Taiwan. Furthermore, a dense GPS profile across the central segment of the Chukou fault

Table 4. Station velocity of Liuchia - Nanhsi GPS profile relative to Paisha.

Station	V_E (mm/yr)	V_N (mm/yr)	V (mm/yr)	AZI (°)
S003	-4.0	2.1	4.5	297.7
S004	-2.6	3.9	4.7	326.3
S007	-13.3	2.7	13.6	281.5
S008	-11.0	3.1	11.4	285.7
S011	-8.9	3.6	9.6	292.0
S012	-36.0	1.2	36.0	271.9
S013	-28.4	5.7	29.0	281.3
S065	-39.6	4.5	39.9	276.5
S066	-33.3	6.9	34.0	281.7
S068	-9.8	0.0	9.8	270.0
S069	-23.9	3.1	24.1	277.4
S070	-16.8	3.8	17.2	282.7
S071	-5.8	2.4	6.3	292.5
0437	-22.0	4.7	22.5	282.1
S082	-10.2	2.9	10.6	285.9
S083	-19.9	1.6	20.0	274.6
S085	-15.9	0.9	15.9	273.2
S086	-22.9	3.7	23.2	279.2
S087	-13.1	6.4	14.6	296.0
S088	-20.5	6.0	21.4	286.3
S089	-23.2	2.7	23.4	276.6
S090	-25.2	0.7	25.2	271.6
S091	-30.0	4.8	30.4	279.1
S092	-30.6	4.6	30.9	278.5

(CKF) was deployed along the highway from Liuchia to Nanhsi in 1993. The repeated GPS data of this profile from 1993 to 1997 are analyzed to realize how the crustal strain is accumulating in the vicinity of the CKF and to assess the possibility of a forthcoming major earthquake in the Chianan area. The outcome of this study is summarized as follows:

(1) In the offshore area between the Penghu Islands and the southwest coast of Taiwan there is insignificant or very slight deformation.

(2) Slight to moderate contraction rates of 0.22-0.97 μstrain/yr in the E-W to ESE-WNW directions are observed in the Coast Plain area.

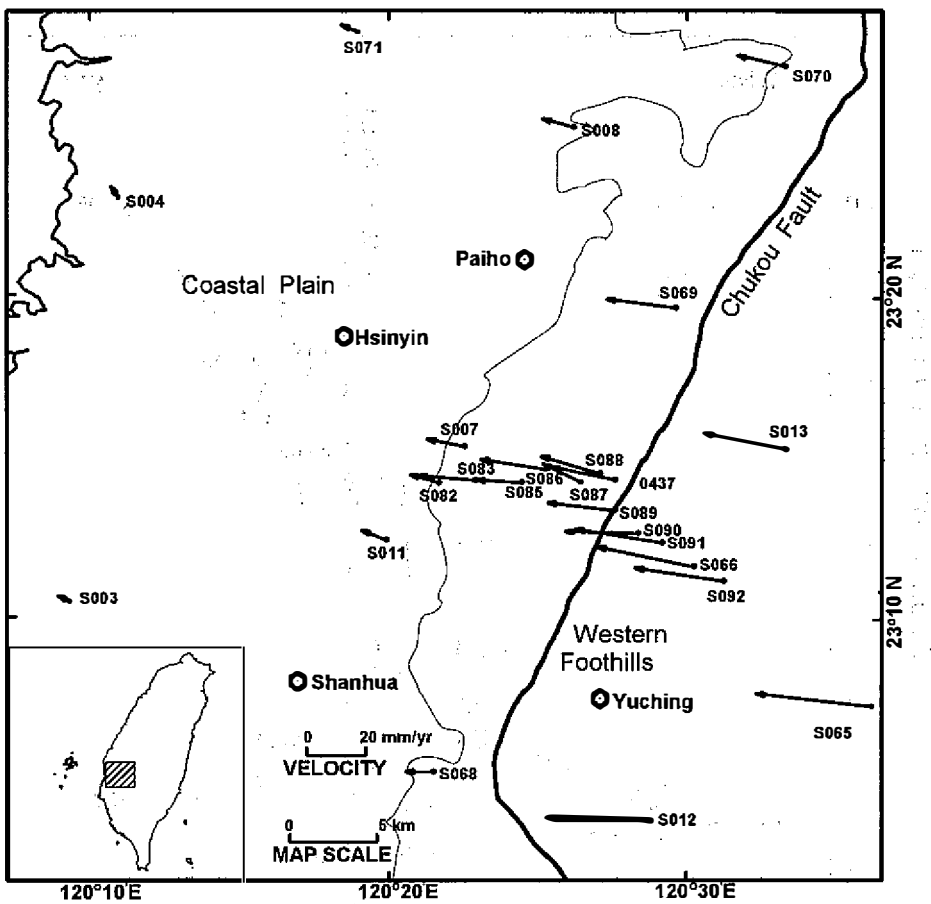

Fig. 10. Station velocities relative to Paisha, Penghu (S01R) for Liuchia-Nanhsi GPS profile and the neighoring stations. Thin line is the approximate boundary between the plain area and the rolling hills.

(3) In the vicinity of the CKF, moderate to remarkable contraction rates of 0.48-2.01 μstrain/yr in 91°-135° are found. Some nets also show significant extension rates of 0.12-1.26 μstrain/yr.

(4) The nets to the east of the CKF have slight to moderate extension rates of 0.06-0.76 μstrain/yr and contraction rates of 0.10-0.58 μstrain/yr. The directions of contraction are mostly in ESE-WNW to SE-NW.

(5) The principal strain rates along the trace of the central and southern segments of the CKF clearly increase toward the south. In contrast, the strain rates along the northern segment of the CKF are more or less at the same level. However, the contraction rates always increase toward the CKF from either the east or the west.

(6) The temporal variations of crustal strain near the CKF are quite uniform during the period from 1990 to 1997. The largest earthquake occurred in the Chianan area after the 1964

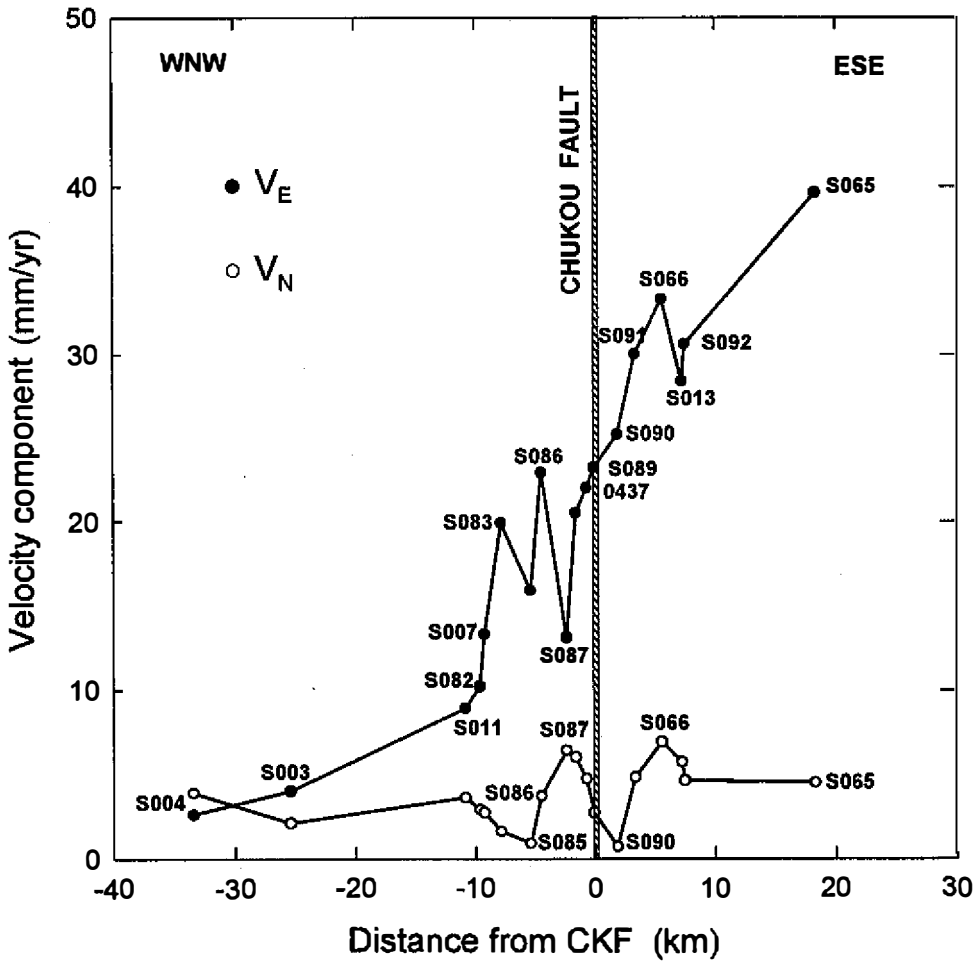

Fig. 11. The east and north velocity components for stations in the central part of Figure 10 plotted as a function of distance from the Chukou fault.

Paiho earthquake, the Tapu earthquake (ML=5.7), did not cause any detectable surface deformation.

(7) Repeated GPS data of the dense profile across the central segment of the CKF indicate that the E-W shortening is distributed at several places and not solely due to slip along the CKF.

(8)The E-W velocity profile shows that the east velocity components relative to Penghu increase dramatically toward the east from 2.6 mm/yr near the coast, to 39.9 mm/yr in the foothill region to the east of the CKF. It implies that the crustal strain is accumulating rapidly in the vicinity of the CKF and there is a high potential of a forthcoming major earthquake.

(9)Since the seismic activity near the southern segment of the CKF is not significant (see Figure 1), the extremely high strain rates here may be due to aseismic slip on the fault. To

verify this inference, densely deployed and frequently surveyed GPS profiles across the CKF as well as detailed geological survey are required.

Acknowledgments We are grateful to many of our colleagues who participated in the GPS field surveys and part-time assistants who collected the continuous GPS data for us. Thanks are also due to our colleagues C. H. Yen and H. H. Su for their assistance in preparing this manuscript and the illustrations and two anonymous reviewers for their valuable comments and suggestions. This study was financially supported by Academia Sinica and the National Science Council of the Republic of China under grant NSC 86-2116-M-001-025.

REFERENCES

Brunner, F. K., and W. M. Welsch, 1993: Effects of the troposphere on GPS measurements. *GPS World*, **4**, 42-51.

Cheng, S. N., and Y. T. Yeh, 1989: Catalog of the earthquakes in Taiwan from 1604 to 1988. Inst. Earth Sci., Academia Sinica, IES-R-661, 255pp.

Chiu, H. T., 1973: Basement rocks under the Neogene formations of west-central Taiwan. *Proc. Geol. Soc. China*, **16**, 51-58.

Chou, J. T., 1969: A petrographic study of the Mesozoic and Cenozoic rock formations in the Tungliang well TL-1 of the Penghu Island, Taiwan China. *Tech. Bull. CCOP ECAFE, U. N.* **2**, 97-115.

Ho, C. S., 1975: An introduction to the geology of Taiwan, explanatory text of the geologic map of Taiwan. The Ministry of Economic Affairs, Taipei, Taiwan, R.O.C., 153pp.

Ho, C. S., 1976: Foothills tectonics of Taiwan. *Bull. Geol. Surv. Taiwan*, **25**, 9-28.

Ho, C. S., 1982: Tectonic evolution of Taiwan : Explanatory text of the tectonic map of Taiwan. Ministry of Economic Affairs, R.O.C., 126pp.

Ho, C. S., 1986: A synthesis of the geologic evolution of Taiwan. *Tectonophysics*, **125**, 1-16.

Hopfield, H. S., 1971: Tropospheric effect on electromagnetically measured range: Prediction from surface weather data. *Radio Sci.*, **6**, 357-367.

Meng, C. Y., 1967: The structural development of the southern half of western Taiwan. *Proc. Geol. Soc. China*, **10**, 77-82.

Prescott, W. H., J. C. Savage, and W. T. Kinoshita, 1979: Strain accumulation rates in the western United States between 1970 and 1978. *J. Geophys. Res.*, **86**, 6067-6072.

Rothacher, M., and L. Mervart (Eds.), 1996: Bernese GPS software v.4.0. Astronomical Institute, University of Berne, Switzerland, 418pp.

Shin, T. C., 1995: Application of waveform modeling to determine focal mechanisms of the 1993 Tapu earthquake and its aftershocks. *TAO*, **6**, 167-179.

Suppe, J., 1980: Imbricate structure of Western Foothills belt, south-central Taiwan. *Petrol. Geol. Taiwan*, **17**, 1-16.

Tsan, S. F., and W. P. Keng, 1968: The Neogene rocks and major structural features of southwestern Taiwan. *Proc. Geol. Soc. China*, **11**, 45-59.

Yu, S. B., and H. Y. Chen, 1994: Global Positioning System measurements of crustal defor-

mation in the Taiwan arc-continent collision zone. *TAO*, **5,** 477-498.

Yu, S. B., H. Y. Chen, and L. C. Kuo, 1997: Velocity field of GPS stations in the Taiwan area. *Tectonophysics*, **274**, 41-59.